DOI 10.2478/ama-2020-0004

AUTOMOTIVE MR SHOCK ABSORBER BEHAVIOUR CONSIDERING TEMPERATURE CHANGES: EXPERIMENTAL TESTING AND ANALYSIS

Łukasz JASTRZĘBSKI*, Bogdan SAPIŃSKI*, Arkadiusz KOZIEŁ*

*Mechanical Engineering and Robotics, Department of Process Control,
AGH University of Science and Technology, Al. Adama Mickiewicza 30, 30-059 Kraków, Poland

lukasz.jastrzebski83@gmail.com, deep@agh.edu.pl, arkadiuszkoziel93@gmail.com

received 21 November 2019, revised 24 March 2020, accepted 27 March 2020

Abstract: This study investigates the automotive magnetorheological (MR) shock absorber behaviour in conditions of changing temperature. Its temperature-dependent behaviour was quantified between ambient and maximal operating temperatures of the device. Aspects addressed include the temperature dependence of the control coil resistance in the absorber, the influence of operating current level on control coil temperature and the temperature dependence of the absorber force response and energy dissipation in the system. The results of experiments enabled us to evaluate the mechanical performance of the absorber at varied temperatures.

Key words: MR Shock Absorber, Temperature, Current, Coil Resistance, Force, Energy

1. INTRODUCTION

Magnetorheological (MR) shock absorbers are used in suspensions of passenger cars and sports vehicles to improve the ride comfort by controlling undesired vibrations. Studies of MR shock absorber behaviour have identified several major determinants of the output force (response), such as mechanical and magnetic hysteresis, control circuit dynamics, driver dynamics, temperature, flow losses, friction and nonlinear relationship between the material's yield stress and the induced flux (Bajkowski and Skalski, 2012; Strecker et al., 2015; Gołdasz et al., 2018; Gołdasz and Sapiński, 2019; Kubik and Gołdasz, 2019). These factors need to be taken into account when designing control systems for the device (Choi et al., 2005; Sims, 2006; McKee et al., 2018). Specifically, there are three key effects of rising temperature on the MR shock absorber force output (Batterbee and Sims, 2009). The first effect involves the reduction of the yield force corresponding to a reduction in the MR fluid's yield stress. The second one is decrease in the slope of the post-yield force–velocity response associated with reduction in the MR fluid's viscosity. The third effect involves the reduction of the force–velocity hysteresis loop size, associated with a change in the absorber's stiffness caused by the ring accumulator pressure.

The present study aims to investigate the temperature factor in the Magnetic Ride absorber in cars of series Audi TT Quatro. This factor is of great importance when the MR device experiences large temperature variations (Gordaninejad and Breese, 1999). The objective of this work is to evaluate the absorber's behaviour under the condition of varied temperature through experiments. The resulting behaviour of the Magnetic Ride absorber will be taken into account by the authors when designing temperature-sensitive controller.

This study is organised as follows. In Section 2, we provide the characteristics of the Magnetic Ride absorber and test facilities. In Section 3, the experimental procedure is summarised for the experiments conducted in the constant climate cabinet with no piston displacement, and then when the absorber is subjected to a particular excitation via piston displacements and constant current inputs. Section 4 covers the experimental results and discussion of the temperature effects on the absorber behaviour. Conclusions are given in the Section 5.

2. STRUCTURE AND FORCE RESPONSES OF THE ABSORBER

The structural design of the absorber is shown in Fig. 1, which reveals a typical mono-tube flow-mode damper configuration with an annular gap. Geometrical parameters of the device are: piston stroke 178 mm, outer diameter of the cylinder 50 mm, the length with the piston in compression position 381 mm and the length with the piston in rebound position 559 mm. The cylinder is filled with 277 cm^3 of MR fluid. The absorber comprises an accumulator 65 cm^3 in volume, filled with nitrogen. The maximal current in the control coil should not exceed 5 A. The device ought to be operated in the temperatures ranging from −30 °C to 100 °C.

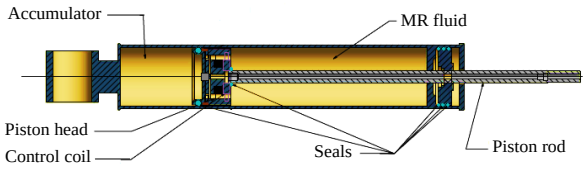

Fig. 1. Schematic diagram

Fig. 2 shows typical plots of force response F vs piston position x (Jastrzębski and Sapiński, 2017). These plots were obtained under

the applied input in the form of triangular piston displacement of amplitude 75 mm and frequency 0.5 Hz, corresponding to the constant velocity of the piston 150 mm/s, both in the rebound phase and in the compression phase. The absorber's force output in the stroke centre position is found to be 335 N at current I = 0 A, whilst under the maximal current I = 5 A in the control coil, the force response is increased 14-fold in relation to that registered under the conditions of no power supply.

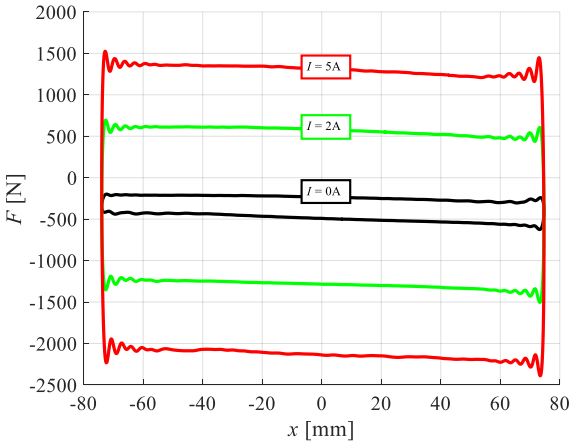

Fig. 2. Force vs piston position

3. TEST FACILITIES AND EXPERIMENTS

In the first stage, the experiments were performed to explore temperature dependence of the control coil resistance in the shock absorber. The experimental setup shown in Fig. 3 comprises an SB11/160/80 constant climate chamber manufactured by Weiss Technik (WEISS TECHNIK, 2019) and a Fluke8846A precision resistance multimeter (FLUKE, 2019). The constant climate chamber allows the temperature to be controlled and maintained at a constant level in the range 20 ºC–100 ºC.

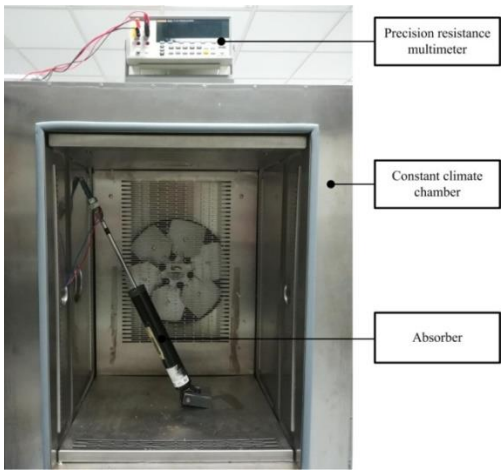

Fig. 3. Test facility with the constant climate chamber

The second cycle of experiments were conducted to determine the relationship between the cylinder temperature in the shock absorber and the temperature of the control coil under the current inputs 1, 2, 3, 4 and 5 A. The case was analysed in which the piston remained immobile at its maximal position in the rebound phase and when it moved at the fixed rate 150 m/s in the compression phase and the rebound phase. The applied triangular input inducing the piston motion around its mid-position had an amplitude A = 75 mm and frequency f = 0.5 Hz. When the applied current levels were 1, 2, 3 and 4 A, the experiment lasted 180 s; with the applied current level at 5 A, the experiment took 480 s (the time required by the cylinder in the shock absorber to reach the temperature of 100 ºC). The cylinder temperature was determined with the use of a thermovision camera, whilst the temperature of the control coil was calculated based on changes in the coil winding's resistance. All experiments were conducted in the test facility shown schematically in Fig. 4 and incorporating an MTS 810 testing system (MTS, 2019) and a current controller (Sapiński et al., 2012), complete with the power supply and the measurement data acquisition system. The current controller is fitted with integrated circuits used for voltage and current measurement in the control coil of the shock absorber and an in-built PID controller. The controller enables the coil to be supplied with currents up to 7 A. Piston displacements and the damping force delivered by the shock absorber were measured with the sensors in the MTS 810 tester machine. The data acquisition system comprises an RT-DAC PCI card (INTECO, 2019) and a PC operated under Windows 7 in the MATLAB/Simulink environment. The temperature of the cylinder in the shock absorber was measured using the Flir E40 thermovision camera (FLIR, 2019).

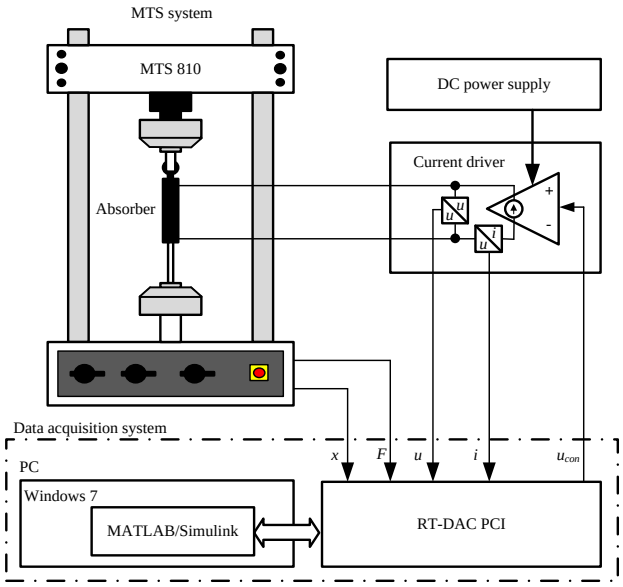

Fig. 4. Test facility with MTS testing system

4. RESULTS AND DISCUSSION

Experimental results summarised in three sub-sections clearly demonstrate how temperature influences the resistance of control coils and how the current level in the coil impacts on the changes in the coil and cylinder temperatures under the condition when the piston should remain immobile, thus revealing the temperature dependence of the mechanical performance of the device.

4.1. Influence of temperature on control coil resistance

The constant climate chamber in which the temperature was maintained constant throughout the experimental procedure is

DOI 10.2478/ama-2020-0004

shown in Fig. 3. Temperature could be varied in the range from 20 °C to 100 °C, at 5 °C intervals. In order to uniformly heat the entire volume of the shock absorber to reach the preset temperature, the absorber was maintained inside the chamber for 1 hour. Afterwards, measurements were taken of the control coil resistance and the temperature inside the chamber was raised at the predetermined rate. The resistance of the cable connecting the absorber with the power drive was duly accounted for in the measurement procedure.

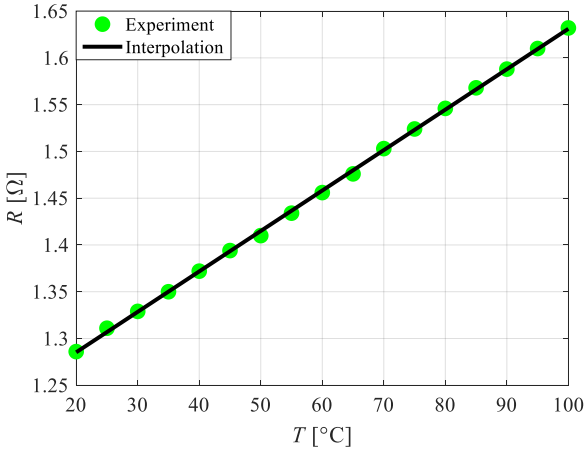

Fig. 5. Coil resistance vs temperature

Experimental data are plotted in Fig. 5. It appears that control coil resistance R is linearly related to the absorber's temperature T. At 20 °C, the coil resistance becomes 1.276 Ω, and at 100 °C, it is found to be 1.643 Ω. Based on the data obtained (indicated in green markers in Fig. 5) and recalling the least square method, the following coefficients were derived accordingly: a = 0.00459 Ω/°C and b = 1.184 Ω of the linear function (see black continuous line), as shown in Equation (1).

$$R = a \cdot T + b \tag{1}$$

For electric conductors, resistance can be expressed as:

$$R = R_0(1 + \alpha \cdot \Delta T) \tag{2}$$

where R_0 is the conductor resistance at the reference temperature T_0, α is the temperature coefficient of resistance and ΔT is the temperature change from T_0 to T.

Recalling Equations (1) and (2), the temperature coefficient of resistance was derived accordingly: α = a/b = 3.88 × 10^{-3} 1/°C. Its value is nearing that listed in physical tables for copper wire from which the control coil is made: α_{CU} = 3.9·× 10^{-3} 1/°C. At T_0 = 0 °C, the calculated coil resistance is: R_0 = b = 1.184 Ω. Temperature T of the coil can be derived recalling Equation (3) and resistance readouts R.

$$T = \frac{1}{\alpha}\left(\frac{R}{R_0} - 1\right) \tag{3}$$

Temperature of the control coil derived from Equation (3) is closer to that of the MR fluid in the gap in the shock absorber than to the temperature on the cylinder surface. An increase in the temperature of MR fluid can be attributed to thermal energy arising due to friction during the fluid flow in the gap and to thermal energy associated with current flow in the control coil.

4.2. Influence of current level on the control coil temperature

Experiments were conducted using the test facility shown in Fig. 4. Throughout the experimental procedure, the piston rod in the shock absorber stayed in the rebound position and remained immobile. Resistance of the control coil R was derived based on the voltage u and current i readouts.

The obtained results are plotted in Figs 6–10. Fig. 6 shows the time histories of the control coil resistance R during heating associated with DC current I. Fig. 7 plots the time history of control coil temperature T, derived from Equation (3).

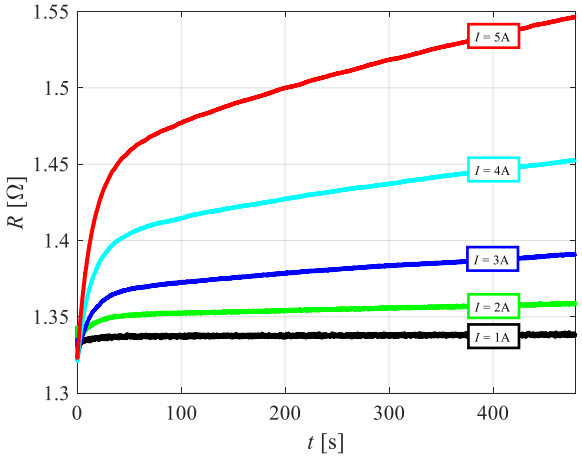

Fig. 6. Time patterns of coil resistance at various current levels

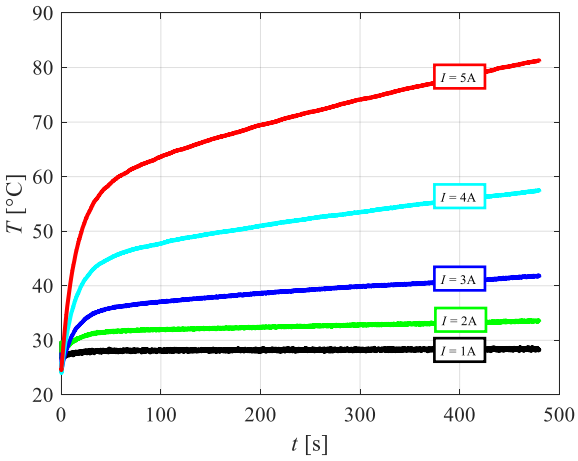

Fig. 7. Time patterns of coil temperature at various current levels

Apparently, after time t = 480 s (current level 1 A), resistance and temperature of the control coil increase by about 1%, whilst at 2 A, there is a 3% increase. It is reasonable to suppose, therefore, that at current levels I ≤ 2A, the released thermal energy will not cause any temperature change of the coil (MR fluid). At current levels 3, 4 and 5 A, resistance and temperature of the control coil increase by 5%, 12% and 20%, respectively. Plots in Figs 6 and 7 clearly indicate that the process of coil heating involves two distinct stages. In the first stage, when t ≤ 50 s, the temperature goes up rapidly; in the second phase, when t > 50 s, the temperature increase is found to be less significant.

To better highlight this effect, plots of coil temperature and

DOI 10.2478/ama-2020-0004

temperature on the cylinder surface vs time are compared for the current level I = 5 A (Fig. 8a). Time histories of the cylinder temperature were derived from the distribution of temperature readouts from the thermovision camera registered in 5-s time intervals. Figs 9 and 10 plot selected temperature distribution patterns registered at the time instants: 0, 50, 240, 480, 540, 600, 720 and 960 s.

Obviously, within the time t ≤ 50 s, the difference between the temperature of the control coil and that of the cylinder tends to grow rapidly. After that time, the temperature difference becomes 35 ºC and remains at that level until the end of the heating phase (t = 480 s). Fig. 8b shows the change in the coil and cylinder temperature from the moment heating of the shock absorber should cease (i.e. from the time instant t = 480 s until t = 960 s). In order that the resistance of the control coil can be derived so as to determine its temperature through voltage u and current i measurements (Fig. 4), the current driver value must be I = 0.5 A. Such current levels should not cause any increase in the control coil temperature (Fig. 7). Apparently (see Fig. 8b), the difference between the temperature of the control coil and that of the cylinder tends to decrease from t = 480 s to t = 530 s. In the subsequent time instants, the temperatures of the control coil and of the cylinders are nearly identical.

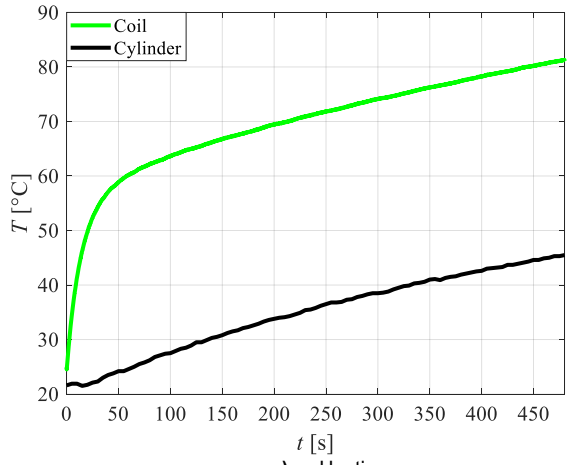

a) Heating

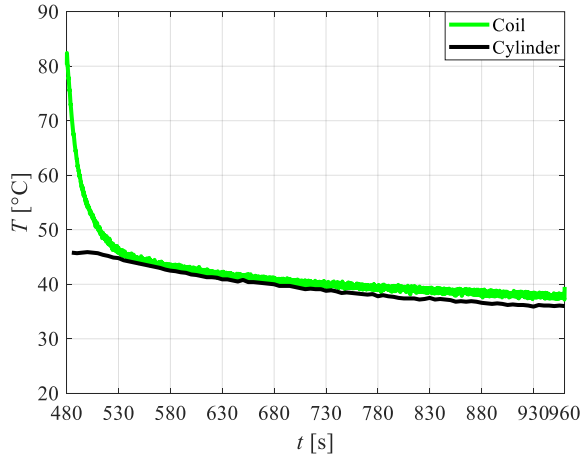

b) Cooling

Fig. 8. Time pattern of the coil and cylinder temperature

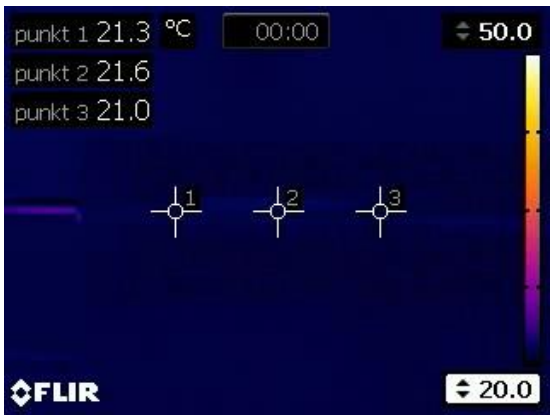

a) t = 0 s

b) t = 50 s

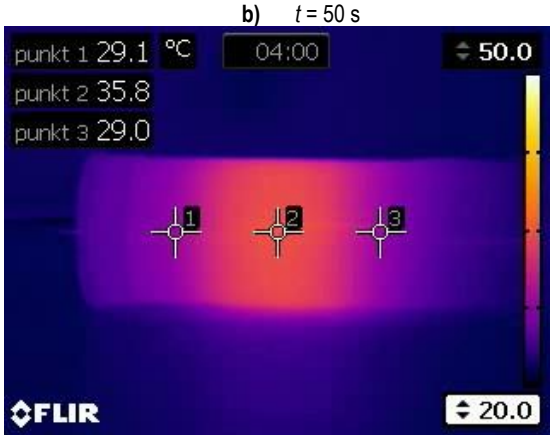

c) t = 240 s

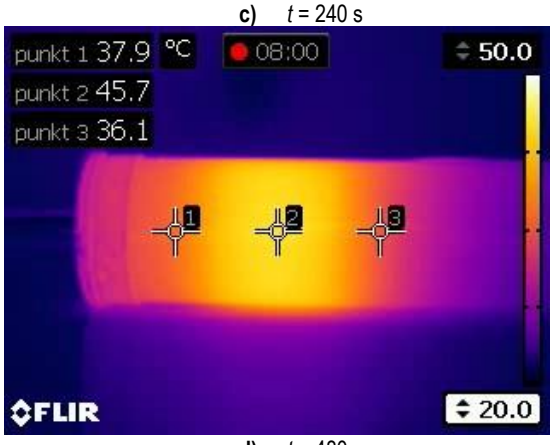

d) t = 480 s

Fig. 9. Temperature distribution on the cylinder surface when heating

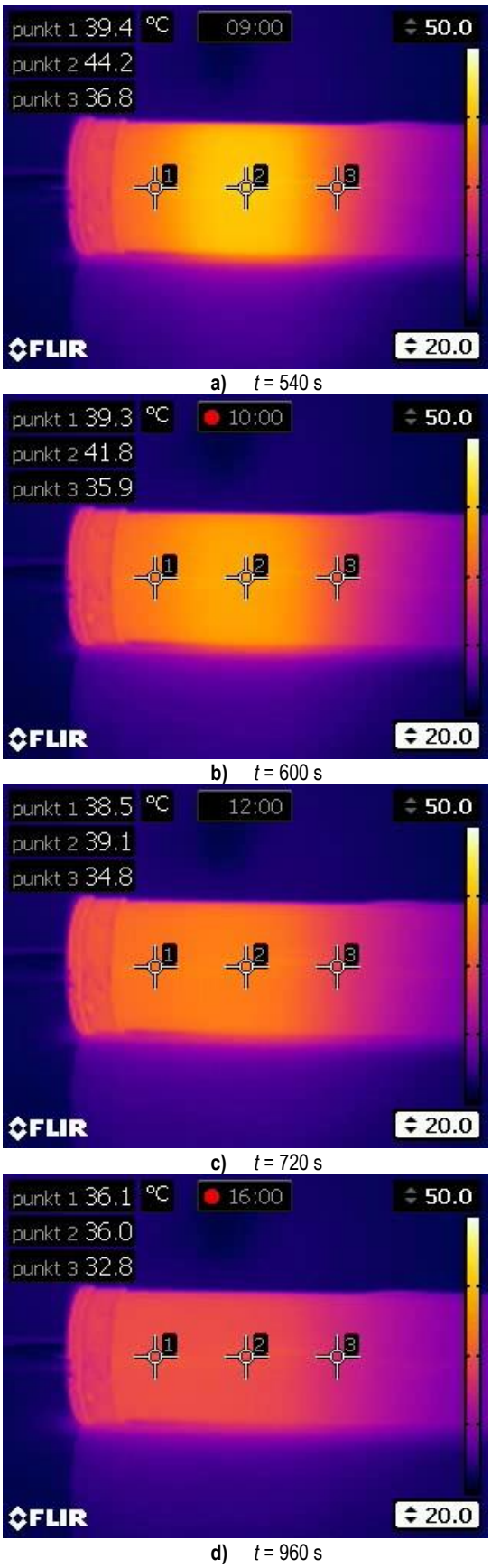

Fig. 10. Temperature distribution on the cylinder surface when cooling

Fig. 9 shows the temperature distribution on the cylinder surface whilst the control coil is heated by the flowing current I = 5 A. The range of camera-registered temperature was set to fall in the interval from 20 ºC to 50 ºC, which affords us the means to highlight the temperature readouts collected at points 1, 2 and 3 A on the surface of the cylinder. Point 2 is located in the middle section of the cylinder surface, which coincides with the mid-point of the piston. Points 1 and 3 lie along the line coinciding with the shock absorber axis, beyond the area in which the piston is located. The temperature of the shock absorber when the piston begins to be heated is 21.6 ºC (Fig. 9a, point 2). Temperature distribution on the surface of the cylinder is uniform, and the temperature difference between points 2 and 3 should not exceed 0.6 ºC. After time t = 50 s, a high-temperature region is revealed on the cylinder surface, its temperature approaching 24.2 ºC (Fig. 9b, point 2). The difference in temperature between points 2 and 3 goes up to 2.4 ºC. After the elapse of 240 s, the temperature at point 2 reaches the level 35.8 ºC (Fig. 9c), and after 480 s, it becomes 45.7 ºC (Fig. 9d). After these time instants, the respective temperature difference between points 2 and 3 would be 6.8 ºC and 9.6 ºC.

Cooling of the control coil is illustrated in Fig. 10. Actually, the temperature at point 2 is 44.2 °C after time t = 540 s, 41.8 °C after t = 600 s, 39.1 °C after t = 720 s and 36 °C after t = 960 s.

4.3. Influence of temperature on the absorber performance

Like the previous case, the experiments were conducted in the setup shown in Fig. 4. Throughout the experimental procedure, the rate of piston motion in the shock absorber was 150 mm/s, both during the compression and the rebound phases. The main purpose of the experiments was to find out how the temperature of the control coil impacts on the shock absorber efficiency and performance in terms of the output force range, response force of the accumulator, dissipated power and energy. Another issue addressed was the temperature dependence of electric power required to supply the control coil with preset DC current. Shock absorber efficiency is derived based on the coil temperature because its value is closer to the temperature of MR fluid than to that of the cylinder surface.

Fig. 11 plots the time histories of the control coil temperature in the course of its heating due to the current flow and friction associated with MR current flow in the gap. After the time instant t = 180 s, temperature of the control coil for the current levels 1, 2, 3, 4, 5 A went up by 27%, 66%, 108%, 153% and 200%, respectively. Time histories of the control temperatures registered for the current level 5 A are compared in Fig. 12, having relevance to the case when the piston was in motion (black line) and remained immobile (red line). Apparently, after the elapse of t = 480s, the control coil temperature became higher by nearly 60 °C whilst the piston was in motion than when it remained immobile. In both cases, the rate of temperature change was enhanced when t ≤ 50 s.

The temperature dependence of the force output of the shock absorber was investigated by varying the control temperature from 30 ºC do 143 ºC (this temperature corresponds to the maximal temperature of the cylinder given in the manufacturer's specification as 100 °C). In order to ensure such range of temperature control, the experiments were conducted with the maximal velocity of the piston motion achievable in the MTS testing system and for the maximal rod displacements both in the compression and the rebound phases (150 mm), under the maximal current level in the control coil 5 A. In those conditions, the cylinder reached a temperature of 100 °C after time t = 480 s.

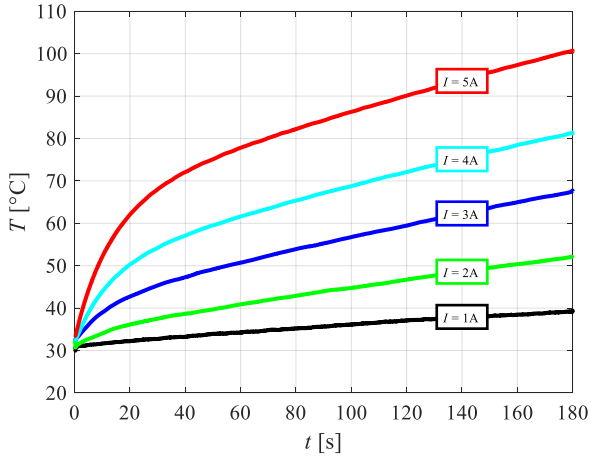

Fig. 11. Time pattern of coil temperature at various current levels; piston excitation A = 75 mm, f = 0.5 Hz

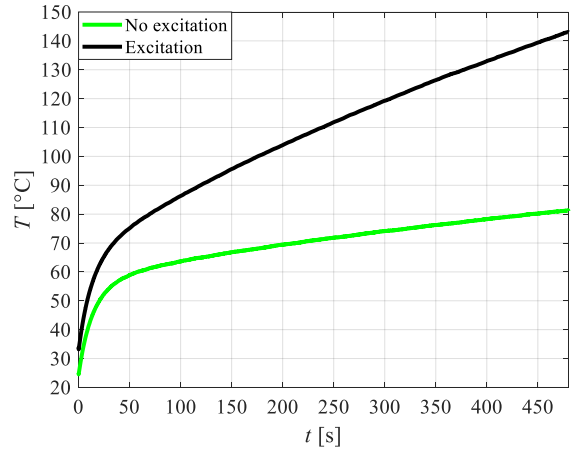

Fig. 12. Time pattern of coil temperature at current I = 5 A with excitation and with no excitation

Fig. 13 shows the force–position loops of the absorber for the respective coil temperatures: 30 °C, 110 °C, 140 °C. An increase in temperature causes reduction of the range of output force, expressing the difference between the force responses when the piston is in the position x = 0 mm in the compression and rebound cycle. At temperatures 30 °C, 110 °C and 140 °C, the respective output force ranges become 3720, 3195 and 2985 N. Temperature dependence of the averaged absorber force response Fm is shown in Fig. 14. Apparently, the magnitude of force response Fm changes by 50% when the control coil temperature goes up from 30 °C to 140 °C, which is attributable to the increase of gas temperature in the accumulator.

Fig. 15 plots the time history of dissipated energy E within a full cycle of the piston motion (the piston returning to its initial position), derived from Equation (4).

$$E(t) = \oint F(x)dx = \int_{t}^{t+\tau} F(t)\frac{dx}{dt}dt \qquad (4)$$

where τ = 1/f.

Apparently, the amount of energy dissipated varies in time, which is associated with temperature increase in the system. The dissipated energy tends to decrease at a faster rate within time t ≤ 50 s than at the remaining time of the experiment. The coil temperature dependence of dissipated energy is plotted in Fig. 16. This relationship can be well approximated by a linear function. In this case, the coefficient of determination r^2 is equal to 0.985. When the temperature of the control coil increases by 110 °C, the amount of dissipated energy will decrease by about 20%.

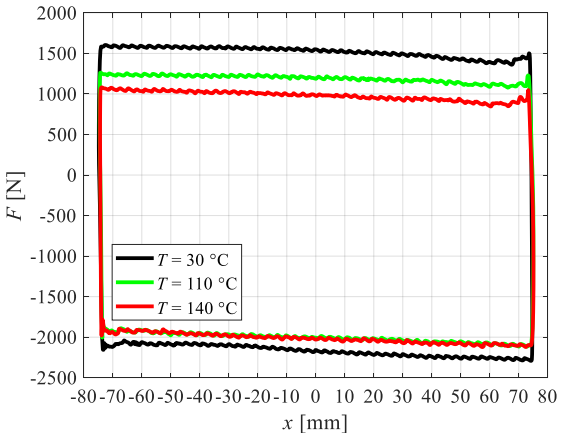

Fig. 13. Force vs piston position at various coil temperatures; piston excitation A = 75 mm, f = 0.5 Hz, current I = 5 A

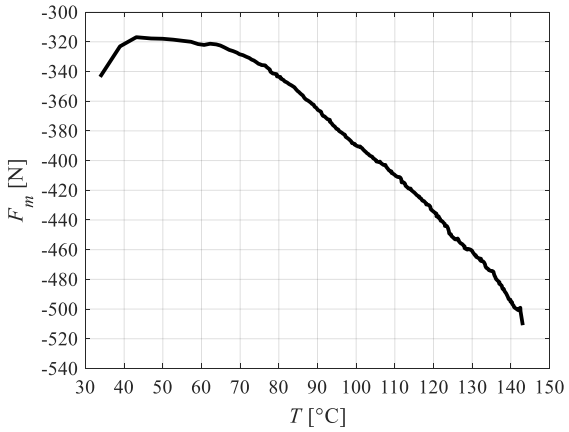

Fig. 14. Force mean value vs coil temperature; piston excitation A = 75 mm, f = 0.5 Hz, current I = 5 A

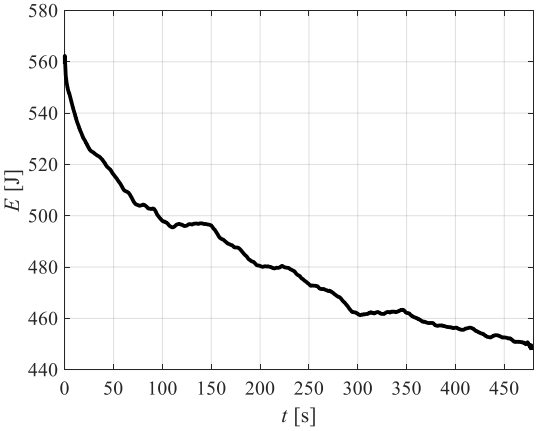

Fig. 15. Time pattern of dissipated energy; piston excitation A = 75 mm, f = 0.5 Hz, current I = 5 A

Fig. 17 gives the plots of average dissipated power and instantaneous electric power supplied to the control coil, in the function of time. Like the dissipated energy (Fig. 15), the average dissipated power P_m tends to decrease, which is attributable to increase in the MR fluid temperature. In order to maintain a constant current level in the control coil whilst its resistance R increases with time, it is required that the power P_{el} supplied from

the current driver should be increased. In the course of the experiment, the temperature of the control coil rose by 110 ºC, which caused a 20% reduction of the averaged dissipated power P_m and a 38% increase of electric power P_{el} supplied to the control coil.

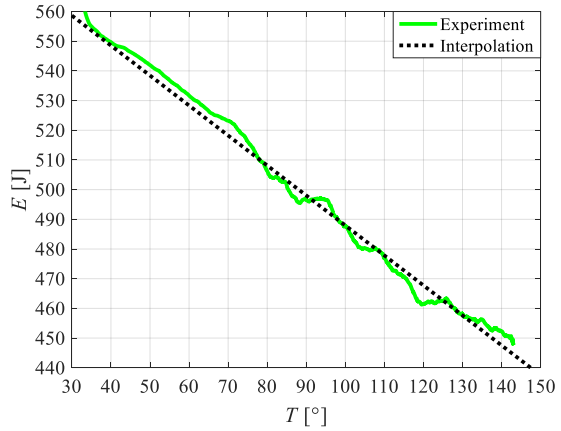

Fig. 16. Dissipated energy vs coil temperature; piston excitation A = 75 mm, f = 0.5 Hz, current I = 5 A

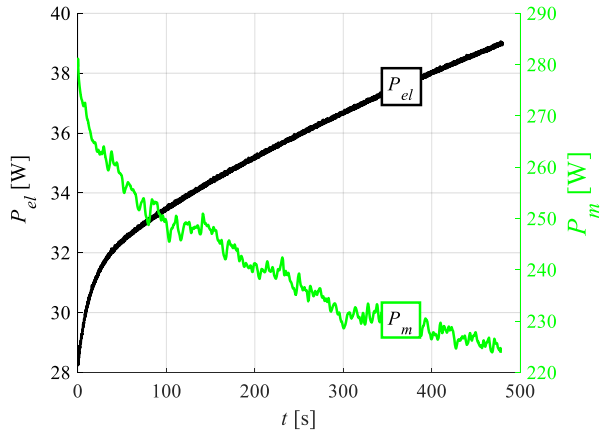

Fig. 17. Time patterns of electrical and mechanical power; piston excitation A = 75 mm, f = 0.5 Hz, current I = 5 A

5. SUMMARY

The study investigates the temperature dependence of the Magnetic Ride absorber behaviour, focusing on the following aspects: temperature dependence of control coil resistance in the device, the influence of operating current on control coil temperature and temperature dependence of force response and energy dissipated in the system.

The experimental results led us to the following conclusions:

- Resistance of the control coil is found to be linearly related to temperature, hence the coil temperature can be established through direct measurements of voltage and current levels.
- When no excitations are applied, thermal energy released by the flow of current less than 2 A will not significantly affect the coil temperature, whilst for the current level 5 A, after 50 s, the difference between the coil temperature and that of the cylinder would approach 35 ºC.
- At currents in excess of 2 A, the rate of coil temperature increase is significantly reduced after 50 s, no matter whether the piston was in motion or remained immobile.
- At a current level 5 A and piston motion velocity 150 mm/s, thermal energy released within the time period of 180 s caused the coil temperature to increase threefold.
- When the coil temperature went up from 30 ºC to 140 ºC, the absolute value of the average absorber force response increased by 50%, which was attributable to an increase in the temperature of gas in the accumulator.
- Under the same conditions, a nearly 20% decrease of dissipated energy and power was registered, whilst the electric power demand increased by 38%.

REFERENCES

1. **Bajkowski J., Skalski P.** (2012), Analysis of Viscoelastic Properties of a Magnetorheological Fluid in a Damper, Acta Mechanica et Automatica, 6(3), 5–410.
2. **Batterbee D., Sims N. D.** (2009), Temperature Sensitive Controller Performance of MR Dampers, Journal of Intelligent Material Systems and Structures, 20, 297–309
3. **Choi S. B., Han S. S., Han Y. M.** (2005), Vibration Control of a Smart Material Based Damper System Considering Temperature Variation and Time Delay, Acta Mechanica, 180(1–4), 73–82.
4. **FLIR Systems Inc.** (2019), *User's manual FLIR Exx series,* Technical Documentation ,https://www.flir.eu
5. **FLUKE Corp.** (2019), *8845A/8846A Digital Multimeter. Users Manual.* Technical Documentation, http://www.fluke.com
6. **Gołdasz J., Sapiński B.** (2019), Influence of temperature on the MR squeeze-mode damper, Proceedings of 20th International Carpathian Control Conference ICCC 2019.
7. **Gołdasz J., Sapiński B., Jastrzębski Ł.** (2018), Assessment of the Magnetic Hysteretic Behaviour of MR Dampers through Sensorless Measurements, vol. 2018, Article ID 3740208, 21 pages.
8. **Gordaninejad F., Breese D. G.** (1999), Heating of Magnetorheological Fluid Dampers, Journal of Intelligent Material Systems and Structures, 10(8), 634–645.
9. **INTECO Ltd.** (2019), *RT-DAC4/PCI Multi I/O board. User's Guide*, Technical Documentation, http://www.inteco.com.pl
10. **Jastrzębski Ł., Sapiński B.** (2017), Experimental Investigation of an Automotive Shock Absorber, Acta Mechanica et Automatica, 11(4), 253–259.
11. **Kubik M., Gołdasz J.** (2019), Multiphysics Model of an MR Damper including Magnetic Hysteresis, Shock and Vibration, Article ID 3246915, 20 pages.
12. **McKee M., Gordaninejad F., Wang X.** (2018), Effects of temperature on performance of compressible magnetorheological fluid suspension systems, Journal of Intelligent Material Systems and Structures, 29(1), 41–51.
13. **MTS System Corp.** (2019), *MTS 810 & 858 Material Testing Systems,* Technical Documentation, http://www.mts.com
14. **Sapiński B., Jastrzębski Ł., Rosół M.** (2012), Power amplifier supporting MR fluid-based actuators, Proceedings of 13th International Carpathian Control Conference ICCC 2012, 612–616.
15. **Sims N. D.** (2006), Limit Cycle Behaviour of Smart Fluid Dampers under Closed-loop Control, Journal of Vibration and Acoustics, 128(4), 413–428.
16. **Strecker Z., Roupec J., Mazurek I., Klapka M.**, (2015), Limiting factors of the response time of the magnetorheological damper, International Journal of Applied Electromagnetics and Mechanics, 47(2), 541–550.
17. **WEISS TECHNIK.** (2019), Climate Test Chamber, Technical Documentation, https://www.weiss-technik.com

This work is supported by AGH University of Science and Technology under research programme No. 16.16.130.942.